2.28 Final Report
Solid Rocket Propellant Combustion

Sam Judd
Email: samjudd@mit.edu

Matthew Vernacchia
Email: mvernacc@mit.edu

1 Introduction

The combustion of solid propellants for rocket propulsion is important because of the long shelf life, high propellant mass fraction, and ease of use of solid motors. Solid propellant motors enable missions that would otherwise be prohibitively difficult because of these unique properties, and are accordingly an important part of rocketry research. Solid propellants have been around since the 13th century, and continue to see significant use currently as hobby rockets and as boosters for many launch systems. Despite this widespread and longtime use, there is much that is still unknown about the mechanisms that take place during the combustion of a solid propellant motor. In the following paper, we will first give an overview of the relations behind performance estimation of the solid rocket motor and explore a basic model for the combustion of a solid propellant as well as a more state-of-the-art model. Following that, we will explore computational alternatives and motivate the development of a computational tool to better understand the effect of the solid fuel selection on the conditions in a combustion chamber.

2 Performance Metrics for Solid Rocket Propulsion Systems

The key performance metric for rocket propulsion systems is Δv, the change in velocity which the propulsion system can impart to the vehicle. Space launch vehicles require a Δv of about $10\,\mathrm{km\,s^{-1}}$, while tactical missiles require about $1\,\mathrm{km\,s^{-1}}$ [1]. The Tsiolkovsky rocket equation defines Δv as:

$$\Delta v = v_e \ln\left(\frac{m_{inert} + m_{prop}}{m_{inert}}\right) \tag{1}$$

Where v_e is the velocity at which exhaust is expelled from the rocket, m_{prop} is the mass of burnable propellant, and m_{inert} is the mass of inert vehicle components (structure, electronics, payload, etc.). To maximize Δv, the exhaust velocity v_e should be as large as possible, and the inert mass fraction $\frac{m_{inert}}{m_{inert}+m_{prop}}$ should be as small as possible.

The choice of propellant influences both terms in the Tsiolkovsky rocket equation. Selecting a denser propellant reduces the required volume of the propulsion system, which in turn reduces the inert structural mass. The exhaust velocity, v_e, can be related to the combustion properties of the propellant. Assume that the process of expansion through the rocket nozzle is adiabatic. The stagnation enthalpy in the combustion chamber must then equal the stagnation enthalpy at the nozzle exit.

$$h_c + \frac{1}{2}v_c^2 = h_e + \frac{1}{2}v_e^2 \tag{2}$$

Now assume that the velocity in the combustion chamber is negligible, $v_c \approx 0$.

$$v_e = \sqrt{2(h_c - h_e)} \tag{3}$$

Further assume that the expansion is isentropic, and that the exhaust gas is ideal and has constant specific heat. The exhaust velocity can then be re-written in terms of the propellant flame temperature T_c, the molar mass of the exhaust $\mathcal{M}$, the exhaust gas ratio of specific heats $\gamma = c_p/c_v$, and the pressure expansion ratio p_e/p_c.

$$v_e = \sqrt{\frac{2\gamma}{\gamma - 1}\frac{\mathcal{R}}{\mathcal{M}}T_c\left(1 - \left(\frac{p_e}{p_c}\right)^{(\gamma-1)/\gamma}\right)} \tag{4}$$

$\mathcal{R} = 8.314\,\mathrm{J\,K^{-1}\,mol}$ is the ideal gas constant. Raising the combustion temperature T_c and lowering the exhaust molar mass $\mathcal{M}$ will increase v_e. Differences in γ between different propellants typically have a small effect on v_e [1].
Typically the efficiency of a propulsion system will be reported using the specific impulse, I_{sp}. Specific impulse is a measure of fuel efficiency, it is defined as the thrust force

divided by the weight of propellant burned per second.

$$I_{sp} = \frac{F}{\dot{m} g_0} \tag{5}$$

Where F is the thrust force and $\dot{m}$ is the mass flow rate of exhaust. Dividing by $g_0 = 9.81\,\mathrm{m\,s^{-2}}$ gives I_{sp} in units of seconds, which is convenient for communication between teams using SI and US customary units. Very high performance liquid propellant rockets achieve an I_{sp} of about 450 s, and typical solid propellant rockets have 200–270 s [1]. I_{sp} is related to the exhaust velocity, and under certain assumptions:

$$I_{sp} = \frac{v_e}{g_0} \tag{6}$$

The specific impulse can be divided into two performance parameters, the thrust coefficient C_F and the characteristic velocity c^*.

$$I_{sp} = \frac{C_F c^*}{g_0} \tag{7}$$

The thrust coefficient is a function of the nozzle expansion parameters: the pressure ratio p_e/p_c, the area ratio $A_t e/A_t$ and the ambient pressure p_a. The characteristic velocity is a function of the combustion parameters: combustion temperature, exhaust molar mass, and the exhaust gas ratio of specific heats γ.

$$C_F = f(p_c, \quad p_e, \quad p_a, \quad A_e/A_t) \tag{8}$$

$$c^* = \sqrt{\frac{\mathcal{R} T_c}{\gamma \mathcal{M}}} \left(\frac{2}{\gamma+1} \right)^{\frac{-(\gamma+1)}{2(\gamma-1)}} \tag{9}$$

Because c^* is independent of the nozzle expansion parameters, it can be used to compare the performance of propellants which are used in different rockets with different nozzles. However, less c^* data is published than I_{sp} data.

In summary, the desired properties of a solid rocket propellant are:

1. High density.
2. High I_{sp} or c^*, which is achieved by:
   (a) High combustion temperature.
   (b) Low molar mass of exhaust products.

3 Chemical Formulations of Solid Rocket Propellants

3.1 Homogeneous Propellants

Homogeneous propellants have spatially uniform composition, and contain oxidizer and fuel fragments within a single molecule. Typically the main component is a nitropolymer (hydrocarbon polymer with $O-NO_2$ groups), with additives to improve the shelf life, mechanical properties, and burning rate [2]. The most popular homogenous propellant is double-base propellant. Double base propellant consists of solid nitrocellulose gelatinized with a liquid energetic nitrate ester, usually nitroglycerin [2].

The combustion of double base propellants produces no visible smoke, which is useful for certain military applications [1]. However, the density and specific impulse of double base propellants is lower than that of composite propellants. Double base propellants were widely used in the 1940s and 50s, but have since been superseded by higher-performance composite propellants [3].

Table 1. Performance of solid propellants. Black powder data from [2], other data from [1]. I_{sp} data assumes ideal expansion from 6.9 MPa to 0.1 MPa.

Formulation	I_{sp}	Flame Temp.	Density
Double base (DB)	220–230 s	2550 K	$1600\,\mathrm{kg\,m^{-3}}$
AN/Polymer	180–190 s	1550 K	$1470\,\mathrm{kg\,m^{-3}}$
AP/Polymer/Al	250–270 s	3440 K	$1800\,\mathrm{kg\,m^{-3}}$
AP/DB/Al	260–265 s	3880 K	$1800\,\mathrm{kg\,m^{-3}}$
Black powder	60–150 s	2300 K	$1600\,\mathrm{kg\,m^{-3}}$

3.2 Composite Propellants

Composite propellants are a heterogeneous mixture of oxidizer and fuel chemicals. Typically the oxidizer is a crystalline salt, and the fuel is a hydrocarbon polymer. The polymer is referred to as a binder, because it holds the oxidizer crystals together and provides the mechanical strength of the propellant [1]. Aluminum or magnesium metal powders may be added as additional fuel to increase the flame temperature.

3.2.1 Oxidizers

Potassium nitrate (KNO_3), ammonium nitrate (NH_4NO_3, AN), and ammonium percholrate (NH_4CLO_4, AP) are common oxidizers [2]. AP has the highest flame temperature and specific impulse, and is the most widely used crystalline oxidizer. However, AP produces exhaust containing HCl, which is toxic, corrosive, and produces visible smoke [1].

AN based propellants have a lower flame temperature and specific impulse and burn more slowly than AP based propellants [1]. AN is used in gas generators, where its slow burning, low flame temperature, and non-corrosive exhaust are beneficial.

Nitramines explosives such as HMX or RDX can also be used as oxidizers. When mixed with polymer binders in the correct ratio, nitramines can produce exhaust which is free of CO_2 and H_2O. The absence of CO_2 and H_2O greatly reduces the infrared signature of the exhaust, which

is valuable for certain military applications [2].

3.2.2 Binders

Binders are usually liquid polymers which can be mixed with solid oxidizer and metal particles, cast, and cured into a rubber-like solid. Polyurethane, polyvinylchloride, polybutadiene acrylonitrile acrylic acid, carboxyl-terminated polybutadiene and hydroxyl-terminated polybutadiene (HTPB) have been used as binders [1], Of these, HTPB is preferred because enables higher solids loading, which leads to a closer to stoichiometric oxidizer to fuel ratio [1].

Uncured HTPB is a oligomer of butadiene. The butadiene monomers are linked at the 1,4 carbons in a cis or trans configuration, or at the 1,2 carbons to form a vinyl group branching off from the main chain [4].

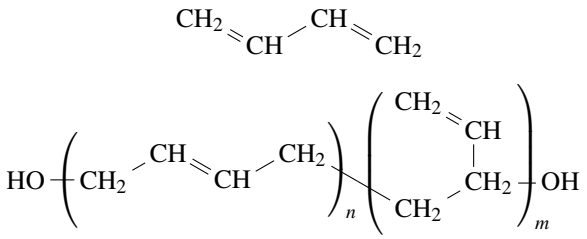

Fig. 1. The 1,3-butadiene monomer and the HTPB oligomer. The oligomer has n cis and trans units and m 1,2 vinyl units. Note that the cis/trans and vinyl units may be interspersed. In typical propellant-grade HTPB $m+n \approx 45$ and $m/n \approx 0.3$ [4].

At room temperature, HTPB is a viscous liquid. After the addition of solid propellant ingredients, the HTPB is cured into a solid via a cross linking reaction. Diisocyanates are used as curatives. An isocyanate $-\mathrm{N{=}C{=}O}$ group reacts with a hydroxyl group to create a urethane bond [4]. Diisocyanates have two isocyanate groups and can bond to two hydroxyl groups, creating a cross link between two HTPB chains.

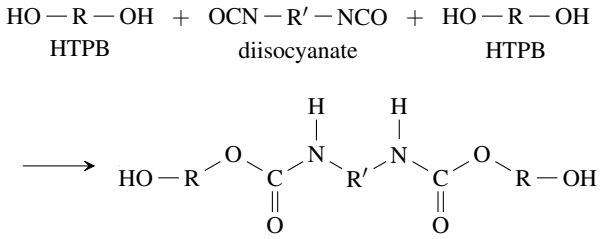

Fig. 2. Cross linking reaction between HTPB and diisocyanate.

Energetic materials, such as glycidyl azide polymer (GAP), can also be used as binders. This provides a slight increase in specific impulse compared to HTPB binder [2].

3.3 Composite Modified Double Base Propellants

Composite modified double base (CMDB) propellants are a heterogeneous mixture of solid oxidizer particles in a double base nitropolymer binder. Unlike normal composite propellants, the binder contains oxidizing $\mathrm{O-NO_2}$ groups, and can burn on its own. Particles of AP or nitramines (HMX or RDX) are mixed into the binder [2].
CMDB propellants offer high density and specific impulse, and have a very high flame temperature. However, they have worse shelf life than AP/polymer composite propellants, and require the handling of hazardous explosives (nitroglycerin, HMX, RDX) during manufacturing.

3.4 Black Powder Propellant

Black powder is a mixture of potassium nitrate ($\mathrm{KNO_3}$), charcoal and sulfur. It was the original rocket propellant used by the Chinese (13th century), the India kingdom of Mysore (18th century) and the British (19th century) [5]. Black powder has very low performance as a rocket propellant, but is cheaper to produce than the other propellants. Today it is only used in applications such as fireworks and model rockets, where low cost is more important that performance [2].

4 Models for Propulsion System Design

The preliminary design of a solid rocket propulsion system uses simplified models which neglect the details of the combustion process.

4.1 Temperature and exhaust composition

Once a propellant is selected, the combustion temperature T_c and exhaust properties γ and $\mathcal{M}$ must be determined. This is typically done with chemical equilibrium software, such as NASA's Chemical Equilibrium with Applications (CEA) program [6]. T_c, γ and $\mathcal{M}$ can also be predicted using experimental data from similar propellants. In preliminary analysis, T_c, γ and $\mathcal{M}$ are assumed to be constant [2].

4.2 Chamber pressure

The equilibrium chamber pressure of a solid rocket motor arises from the balance of exhaust generation from combustion and exhaust discharge through the nozzle. The mass discharge rate is

$$\dot{m}_d = C_D A_t p_c \tag{10}$$

where A_t is the nozzle throat area, p_c is the chamber pressure, and C_D is the nozzle discharge coefficient.

$$C_D = \sqrt{\frac{\mathcal{M}\gamma}{T_c \mathcal{R}} \left(\frac{2}{\gamma+1}\right)^{\frac{\gamma+1}{\gamma-1}}} \tag{11}$$

The mass generation rate is

$$\dot{m}_g = \rho_p A_b r \tag{12}$$

where ρ_b is the density of the solid propellant, A_b is the burning area, and r is the linear burning rate. The burning rate is assumed to have a power-law dependence on pressure (Vieille's Law) [1, 2]:

$$r = ap_c^n \tag{13}$$

where a and n are empirical constants which depend on the propellant. n is unitless and a has units of velocity per (pressure to the nth power).

Now the chamber pressure can be determined. Assume that the exhaust gas is ideal. The chamber pressure depends on the mass of exhaust gas in the chamber.

$$m_c = \frac{p_c V_c}{RT_c} \tag{14}$$

where V_c is the free volume in the chamber and $R = \mathcal{R}/\mathcal{M}$ is the specific gas constant of the exhaust.

The rate of mass accumulation in the chamber is

$$\dot{m}_c = \dot{m}_g - \dot{m}_d \tag{15}$$

Using eqn. 10, 12 and 13, this can be written as a differential equation on the chamber pressure:

$$\frac{V_c}{RT_c}\frac{\mathrm{d}p_c}{\mathrm{d}t} = A_b \rho_b a p_c^n - A_t C_D p_c \tag{16}$$

Eqn. 16 has an equilibrium point at $A_b\rho_b a p_c^n = A_t C_D p_c$.

$$p_{eq} = \left(\frac{A_b \rho_p a}{A_t C_D}\right)^{\frac{1}{1-n}} \tag{17}$$

If $n < 1$, this equilibrium is stable, and p_{eq} is the nominal chamber pressure of the rocket motor. Excess chamber pressure will cause the discharge rate to exceed the generation rate, and p_c will restore to equilibrium. If $n > 1$, the equilibrium is unstable, and the rocket motor will not sustain stable combustion. Excess chamber pressure will cause the generation rate to exceed the discharge rate, and p_c will rapidly increase.

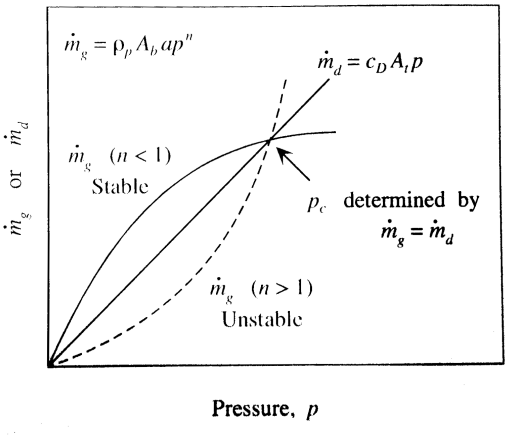

Fig. 3. Mass balance principle and stable burning point in a rocket motor. Reprinted from [2].

The thrust force of the rocket depends on the chamber pressure and the throat area:

$$F = A_t p_c \sqrt{\frac{2\gamma^2}{\gamma-1}\left(\frac{2}{\gamma+1}\right)^{\frac{\gamma+1}{\gamma-1}}\left(1-\left(\frac{p_e}{p_c}\right)^{\frac{\gamma-1}{\gamma}}\right)} + (p_e - p_a)A_t \tag{18}$$

Using eqn. 17 and 18, designers will select values of A_b and A_t which meet the thrust requirement at a reasonable chamber pressure (e.g 5–10 MPa. If the required A_b is too large to be fit within the volume envelope, the designers will change to a faster-burning propellant (e.g. by adding an energetic nitramine) and repeat the design process.

The burn rate parameters a and n in eqn 13 must be determined before a motor can be designed with a new propellant. These are traditionally determined by experiment (see section **??**), but computational combustion models are also being developed.

5 Experimental Techniques

The primary experiment in solid propellant development is the strand burner. The strand burner device is a pressure vessel containing a small rod of propellant [1]. The strand burner is filled with an inert gas, and is regulated to a constant pressure. The propellant is then ignited, and the time taken to burn the length of the rod is measured (see figure 4). By repeating this experiment at several pressures, a correlation between pressure and burning rate can be established. a and n from equation 13 can be found by a power law regression on this data.

6 Models of the Combustion Process

In our modeling the combustion process, we will only examine composite propellants with an Ammonium Perchlorate (AP) oxidizer, as this is the most common propellant formulation used. On a large scale, the combustion can be

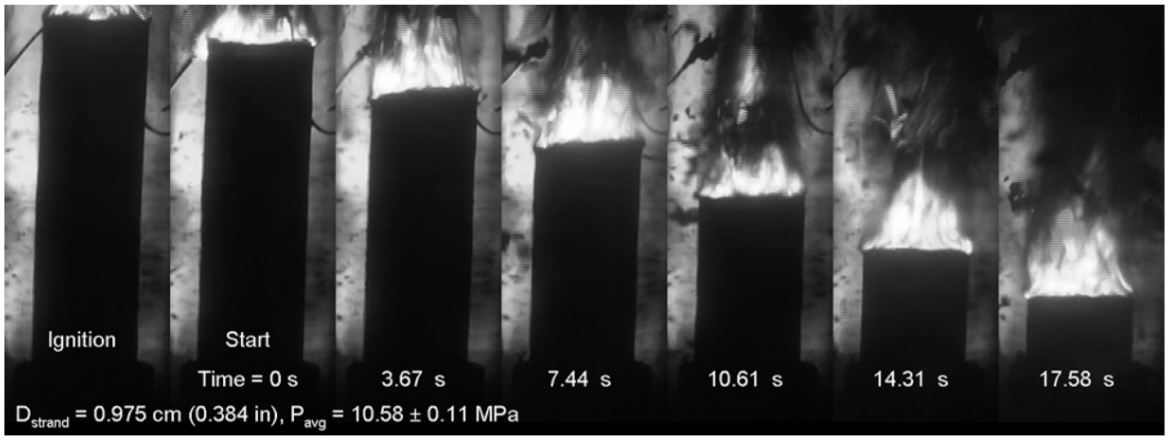

Fig. 4. A propellant rod burning in a strand burner. Reprinted from [7].

analyzed through a relatively simple energy balance at the interfaces between reaction zones, which are detailed in figure 5. At the surface, a decomposition reaction releases gaseous products from the solid propellant. These products mix in zone I, and then burn in zone II.

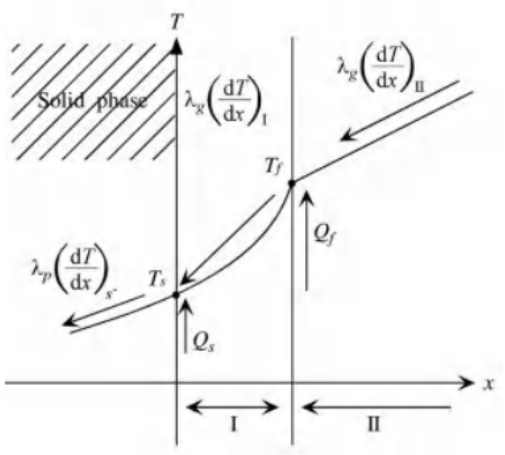

Fig. 5. Zone I is the nonburning preparation zone and II is the exothermic reaction zone. Reprinted from [2].

The energy balances at the solid-I and I-II interfaces can be written as:

$$\lambda_p \frac{dT}{dx}_{s-} = \lambda_g \frac{dT}{dx}_{I} + \rho_p r Q_s \tag{19}$$

$$\lambda_g \frac{dT}{dx}_{I} = \lambda_g \frac{dT}{dx}_{II} + \rho_g r Q_f \tag{20}$$

where λ is the thermal conductivity and Q is the heat of reaction. The Q_s is a negative value at the surface, representing the need to decompose and melt the AP, while the Q_f is positive and correlates to the flame. Therefore, heat flux from the flame through zone I to the surface is required to sustain the reaction. The amount of heat flux to the surface governs the overall rate of the process [2].

Even from this simplified model, if we assume, as Kubota does in [2], that $\lambda_g \frac{dT}{dx}_{II} = 1.71 \times 10^4 p^{0.67}$, then we can see many of the important relations in the system. From this, we can note that heat flux has and exponential dependence on the pressure. We can then see that as the pressure increases, more heat will flow to the solid and thus more will sublimate off, further fueling the reaction. Additionally, if we assume that the flame temperature does not vary strongly with pressure, then we also can note that the flame front will move closer to the wall as the pressure increases, again increasing conduction heat transfer to the wall.

6.1 Solid Decomposition

6.1.1 Decomposition of Ammonium Perchlorate Oxidizer

When heated, AP decomposes into an oxidizer-rich vapor. This vapor reacts exothermically with itself, with a flame temperature of 1200–1400 K [9]. The products of decomposition and of the gas-phase reaction then burn with the products of the binder decomposition.

First, AP undergoes a crystal phase transition from orthorhombic to cubic at 520 K, which is slightly endothermic by 80 kJ kg^{-1} [2,9]. At a high heating rate and high pressure, AP begins to melt at 720 K, and there is a liquid layer on the surface during combustion [2,8,9].

Guirao and Williams [8] propose that the decomposition occurs in two parallel processes. Roughly 70% of the AP melts and decomposes at the surface via condensed-phase reactions. The remainder dissociates into NH_3 and HClO gas, which react with each other in the gas phase.

The gas phase reaction is approximately

$$NH_4ClO_4 \longrightarrow NH_3 + HClO_4 \tag{21}$$

$$NH_3 + HClO_4 \longrightarrow 1.62\,H_2O + 1.015\,O_2 + 0.76\,HCl + 0.265\,N_2 + 0.23\,NO + 0.12\,Cl_2 + 0.12\,N_2O \tag{22}$$

Table 2. Decomposition of solid ingredients in AP/HTPB composite propellant. E and A are the activation energy and pre-exponential factor in the Arrhenius relation. Negative values of heat of decomposition are exothermic. AP data from [2, 8, 9]. HTPB data from [4, 10–12].

Ingredient	Decomp. Temp.	E	A	Heat of Decomp.	Products
AP	607–720 K	gas: $65\,\mathrm{kJ\,mol^{-1}}$ condensed: $244\,\mathrm{kJ\,mol^{-1}}$	gas: $2.03\times10^{11}\,\mathrm{cm^3\,mol^{-1}\,s^{-1}\,K^{-1}}$ condensed: $2.46\times10^{18}\,\mathrm{s^{-1}}$	$-420\,\mathrm{kJ\,kg^{-1}}$	NH_3 $HClO_4$ H_2O HCl O_2 N_2 NO Cl_2 N2O
HTPB	620–700 K	33–70 $\mathrm{kJ\,mol^{-1}}$	$299\,\mathrm{g\,cm^{-2}\,s^{-1}}$	$1800\,\mathrm{kJ\,kg^{-1}}$	C_4H_6 CH_2O CH_n C_2H_n

although the exact equilibrium composition of the products depends on pressure [8]. The gas phase reaction has second-order kinetics given by

$$\frac{\mathrm{d}[\mathrm{HClO_4}]}{\mathrm{d}t} = -k_g[\mathrm{HClO_4}][\mathrm{NH_3}] \tag{23}$$

$$k_g = A_g T e^{\frac{-E_g}{\mathcal{R}T}} \tag{24}$$

with an activation energy of $E_g = 65\,\mathrm{kJ\,mol^{-1}}$ and a pre-exponential factor of $A_g = 2.03\times10^{11}\,\mathrm{cm^3\,mol^{-1}\,s^{-1}\,K^{-1}}$ [8]. A detailed mechanism for the gas phase reaction may be found in [13].

The condensed-phase reaction begins with the breaking of Cl–O bonds in ClO_4^- [8]. This releases oxygen atoms and chloride, which react with NH_4^+ to form NO, H_2O, and HCl [14].

$$2\,\mathrm{ClO_4^-} \longrightarrow \mathrm{Cl_2} + \mathrm{O^{2-}} + 7\,\mathrm{O} \tag{25}$$

$$\mathrm{O^{2-}} + 2\,\mathrm{NH_4^+} \longrightarrow \mathrm{H_2O} + 2\,\mathrm{NH_3} \tag{26}$$

$$2\,\mathrm{NH_3} + 7\,\mathrm{O} \longrightarrow 2\,\mathrm{NO} + 2\,\mathrm{H_2O} + 2\,\mathrm{H} + 1.5\,\mathrm{O_2} \tag{27}$$

$$2\,\mathrm{H} + \mathrm{Cl_2} \longrightarrow 2\,\mathrm{HCl} \tag{28}$$

The reaction is first-order with kinetics given by:

$$\frac{\mathrm{d}[\mathrm{ClO_4}-]}{\mathrm{d}t} = \frac{\mathrm{d}[\mathrm{NH_4^+}]}{\mathrm{d}t} = -k_s[\mathrm{ClO_4}-] \tag{29}$$

$$k_s = A_s e^{\frac{-E_s}{\mathcal{R}T_s}} \tag{30}$$

with an activation energy of $E_s = 244\,\mathrm{kJ\,mol^{-1}}$ and a pre-exponential factor of $A_s = 2.46\times10^{18}\,\mathrm{s^{-1}}$ [8].

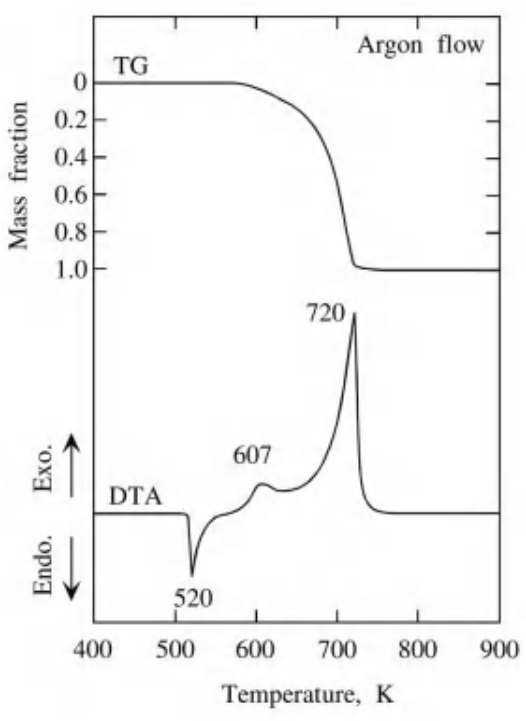

Fig. 6. Thermal decomposition process of AP measured by thermal gravimetry (TG) and by differential thermal analysis (DTA). The sample was heated at a rate of $0.33\,\mathrm{K\,s^{-1}}$. Reprinted from [2]

.

6.1.2 Decomposition of HTPB Binder

When heated HTPB decomposes into a fuel-rich vapor, which then burns with products of the AP decomposition. In cured HTPB, the first reaction is the decomposition of the isocyanate cross links [4]. This occurs via two mechanisms: either the urethane bond is cleaved, releasing isocyanates; or the urethane bond is decarboxylated, releasing CO_2 (see figure 7). The temperature at which isocyanate desorption occurs depends on the boiling point of the isocyanate.

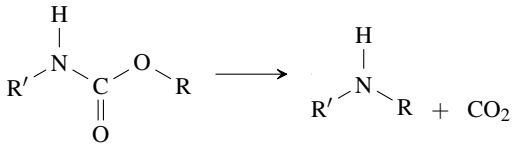

Fig. 7. Decarboxylation of the urethane bond.

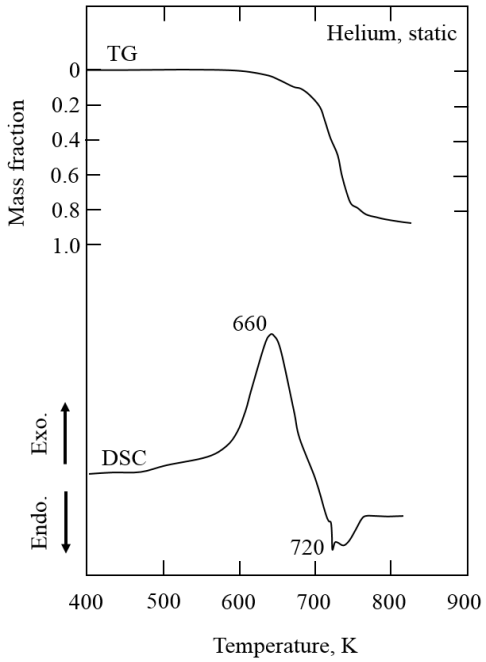

Fig. 8. Thermal decomposition process of HTPB measured by thermal gravimetry (TG) and by differential scanning calorimetry (DSC). The sample was heated at a rate of $0.25\,\mathrm{K\,s^{-1}}$. Data from [10]

.

At slow heating rates, the decomposition of isocyanate is accompanied by cyclization of the HTPB backbone [4]. Cyclization breaks C=C bonds and is therefore exothermic; it is responsible for the exothermic peak at 660 K in figure 8. However, cyclization is relatively slow, and does not occur at faster, combustion-like heating rates (250–350 $\mathrm{K\,s^{-1}}$).

After the decomposition of isocyanate, the HTPB backbone begins to break down at a temperature of about 700 K. [4] observed the products this reaction to be butadiene, 4-vinylcyclohexene (C_8H_{12}, a dimer of butadiene), and CH_2O. However, their products mixed with cool Ar during the observation. In a hotter combustion environment, the larger hydrocarbons would pyrolyze to CH_n and C_2H_n [11].

The activation energy of the overall HTPB decomposition reaction under fast heating is 33–70 $\mathrm{kJ\,mol^{-1}}$ [4, 12]. This relatively low activation energy indicates that desorption, not the breaking of chemical bonds, is the rate-controlling process [4, 12].

The kinetics of the binder decomposition do not have a strong effect on the overall burning rate of the propellant [12, 15].

6.2 AP/HTPB Kinetic Mechanism

Several kinetic mechanisms have been developed for the gas-phase reaction of the vapors evolved from AP and HTPB. The mechanism of Jeppson, Beckstead and Jing is presented in figure 9.

6.3 Flame Structure

The flame structure of composite propellant combustion depends on the heterogeneous distribution of binder and oxidizer on the surface of the propellant. The most basic model analyzes the relatively simple case of a periodic Binder-Oxidizer-Binder sandwich, as shown in Figure 10. This model is bounded on either side by periodic boundaries, so one can imagine the alternating pattern of binder and oxidizer continuing to infinity.

Fig. 10. Sandwich of Binder in between oxidizer crystals.

This represents on the micro scale, a spot of binder between two larger oxidizer particles exposed to the reacting chamber flow or vice-versa, depending on the thicknesses of the layers. Additionally, since the surface recesses with time,

GAS PHASE KINETIC MECHANISM

Reaction	A	b	E_A
1. HCLO4=CLO3+OH	1.00E+14	0.00	39100.0
2. HCLO4+HNO=CLO3+NO+H2O	3.00E+13	0.00	6000.0
3. HCLO4+HCO=CLO3+CO+H2O	5.00E+13	0.00	0.0
4. HCLO4+HCO=CLO2+CO2+H2O	1.50E+12	0.00	0.0
5. CLO3=CLO+O2	1.70E+15	0.50	0.0
6. CL2+O2+M=CLO2+CL+M	6.00E+08	0.00	11200.0
7. CLO+NO=CL+NO2	6.80E+12	0.00	311.0
8. CLOH+CLO=CL2+HO2	1.00E+14	0.00	10000.0
9. CLOH+OH=CLO+H2O	1.80E+13	0.00	0.0
10. HCL+OH=CL+H2O	5.00E+11	0.00	750.0
11. CL2+H=HCL+CL	8.40E+13	0.00	1150.0
12. NH3+CLO=NH2+CLOH	4.24E+11	0.50	6400.0
13. NH3+CL=NH2+HCL	4.50E+11	0.50	100.0
14. NH3+OH=NH2+H2O	5.00E+07	1.60	955.0
15. NH2+O2=HNO+OH	6.00E+09	0.50	0.0
16. NH2+NO=N2+H2O	2.40E+11	0.00	0.0
17. NH2+NO=NNH+OH	6.00E+11	0.00	0.0
18. NNH+NO=HNO+N2	5.00E+13	0.00	0.0
19. HNO+OH=NO+H2O	1.30E+07	1.90	-950.0
20. HNO+O2=NO2+OH	1.00E+13	0.00	10000.0
21. HNO+H=H2+NO	4.50E+11	0.72	660.0
*22. NO+H+M=HNO+M	8.90E+19	-1.32	740.0
23. N2+HO2=HNO+NO	8.00E+10	0.50	41800.0
24. NO+HO2=NO2+OH	2.11E+12	0.00	480.0
25. NO2+H=NO+OH	5.00E+14	0.00	1740.0
26. H2+OH=H2O+H	2.16E+08	1.51	3430.0
27. CH2CO+OH=CH2O+HCO	2.82E+14	0.00	0.0
28. CH2CO+NO2=CH2O+CO+NO	1.00E+13	0.00	6000.0
29. C2H3+O2=CH2O+HCO	3.98E+12	0.00	-240.0
*30. C2H2+H(+M)=C2H3(+M)	5.60E+12	0.00	2400.0
31. C2H2+OH=CH3+CO	4.84E-04	4.00	-2000.0
*32. H2+CO(+M)<=>CH2O(+M)	4.30E+07	1.50	79600.0
33. CH4+CL=CH3+HCL	2.50E+13	0.00	3830.0
34. CH4+CLO=CH3+CLOH	6.00E+11	0.50	5700.0
35. CH4+H=CH3+H2	6.60E+08	1.62	10840.0
36. CH4+OH=CH3+H2O	1.00E+08	1.60	3120.0

Reaction	A	b	E_A
*37. CH3+H(+M)=CH4(+M)	1.27E+16	-0.63	383.0
*38. HCO+M=CO+H+M	1.87E+17	-1.00	17000.0
39. HCN+OH=NH2+CO	1.62E+02	2.56	9000.0
40. CO+OH=CO2+H	4.76E+07	1.23	70.0
41. CO+CLO=CO2+CL	3.00E+12	0.00	1000.0
42. CO+CLO2=CO2+CLO	1.00E+10	0.00	0.0
43. C2H4+OH=H2O+C2H3	3.60E+06	2.00	2500.0
44. C4H6+OH=2C2H2+H2O+H	5.00E+12	0.68	1100.0
45. C4H6+CLO=2C2H2+CLOH+H	5.00E+12	0.50	6400.0
46. C4H6+CL=2C2H2+HCL+H	6.75E+12	0.50	100.0
47. H+O2=O+OH	8.30E+13	0.00	14413.0
48. C2H2+O=CH2+CO	1.02E+07	2.00	1900.0
49. CH2+H2=CH3+H	5.00E+05	2.00	7230.0
*50. CH2+H(+M)=CH3(+M)	2.50E+16	-0.80	0.0
51. CH4+O=CH3+OH	1.02E+09	1.50	600.0
52. CH3+O=CH2O+H	8.43E+13	0.00	0.0
53. CH2+O=H+HCO	8.00E+13	0.00	0.0
54. CH3+O2=OH+CH2O	3.60E+10	0.00	8940.0
55. OH+CH3=CH2+H2O	5.60E+07	1.60	5420.0
56. OH+CH2=H+CH2O	2.00E+13	0.00	0.0
57. CH2+O2=OH+HCO	1.32E+13	0.00	1500.0
58. C2H4+O2=2CO+2H2	1.80E+14	0.00	35500.0
59. O2+HNO=NO+HO2	1.00E+13	0.00	13000.0
60. NH2+NO2=2HNO	2.00E+12	0.00	0.0
61. NH2+CLO=HNO+HCL	2.50E+12	0.00	0.0
*62. H+CL+M=HCL+M	5.30E+21	-2.00	-2000.0
*63. CL+HO2=CLO+OH	2.47E+13	0.00	894.0
64. CLO+O=CL+O2	9.70E+12	0.00	507.0
65. HCL+H=H2+CL	2.30E+13	0.00	3500.0
66. HCL+O=OH+CL	5.24E+12	0.00	6400.0
67. CL2+O=CL+CLO	2.51E+12	0.00	2720.0
*68. N2O(+M)=N2+O(+M)	6.20E+14	0.00	56100.0
69. N2O+OH=N2+HO2	2.00E+12	0.00	21060.0
70. N2O+O=NO+NO	2.90E+13	0.00	23150.0
71. N2O+O=N2+O2	1.40E+12	0.00	10810.0
72. N2O+H=N2+OH	4.40E+14	0.00	18880.0

Note. $k=AT^b\exp(-E_A/RT)$; units for A, b, E_A: cal, mole, sec, cm^3, K. *Reaction includes pressure dependence parameters.

Fig. 9. AP/HTPB composite propellant gas phase kinetic mechanism. Reprinted from [16].

we will adopt a moving coordinate system that moves with the solid surface, so in effect more binder and oxidizer move up as the material burns.

6.3.1 BDP Model of Flame Structure

The first model of solid fuel combustion was put forth by Beckstead, Derr, and Price (BDP) in 1970. This model consists of three flames that form over the surface of the oxidizer, usually taken to be Ammonium Perchlorate (AP). The first flame is a monopropellant flame that forms as the solid propellant is preheated by conduction from the burning gas above. This causes the AP to decompose as outlined in formula 31.

$$NH_4ClO_4 \longrightarrow NH_3 + HClO_4 \tag{31}$$

This flame is dependent completely on kinetics as it does not need to mix in order to react. Then, the second flame is the primary flame which is dominated by mixing between the decomposing oxidizer and binder. This is the primary form of energy release. The oxygen rich products of the monopropellant flame then move upward to form a diffusion flame with all the typical diffusion flame characteristics. These three flames can be seen in Figure 11.

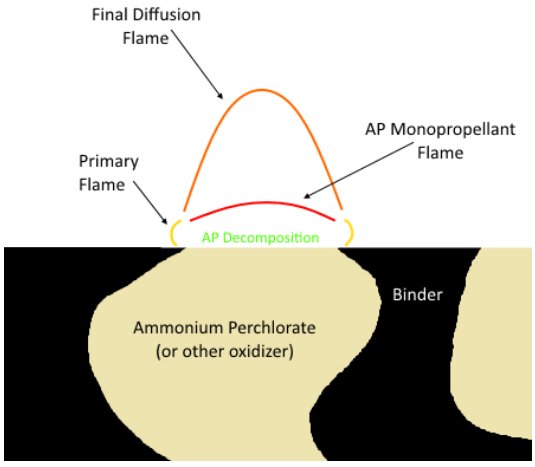

Fig. 11. A section of a solid propellant showing flame structure at low pressure. Adapted from [15].

6.3.2 Surface Temperature of BDP Model

In order to model this flame, the conservation of mass for the flame can be written as as the sum of the fuel mass flux out of the surface and the oxidizer mass flux out of the surface:

$$\dot{m}_{tot} = \dot{m}_f(\frac{S_f}{S_0}) + \dot{m}_{ox}(\frac{S_{ox}}{S_0}) \tag{32}$$

By further requiring that the ratio of oxidizer consumption to fuel consumption over time approach the weight ratio of oxidizer to fuel of the propellant, denoted α, then the equation can be further simplified to the form below.

$$\dot{m}_{tot} = \frac{\dot{m}_f}{\alpha}(\frac{S_f}{S_0}) = \frac{\dot{m}_{ox}}{1-\alpha}(\frac{S_{ox}}{S_0}) \tag{33}$$

Knowing that $\dot{m_{tot}} = \rho_P \dot{r}$, it is clear that either the fuel or the oxidizer mass flux can determine the overall regression rate of the surface. Since the regression of the oxidizer can be assumed to be the dominant characteristic [15], the oxidizer expression for the mass flux is used.

To determine the fraction of the surface that is oxidizer and exposed to reaction, assume that the sections of oxidizer that protrude out of the binder are spherical. Then, the area fraction can be written as

$$\frac{S_{ox}}{S_0} = \frac{\xi[6\frac{h}{D_0}^2 + 1]}{6\xi\frac{h}{D_0}^2 + 1} \tag{34}$$

where ξ is the volume fraction of oxidizer in the propellant and $\frac{h}{D_0}$ is the fractional distance the oxidizer crystal is away from the overall surface, either protruding or recessed. This fraction can be written as

$$\frac{h}{D_0} = \frac{1}{2}(1 \pm \frac{1}{\sqrt{3}})(1 - \frac{\dot{r}_{ox}}{\dot{r}_f}) + \dot{r}_{ox}\frac{t_{ign}}{D_0} \tag{35}$$

where the last term depends on the ignition time of the fuel. This relation combined with relation 34 and the Arrhenius rate term for the oxidizer mass flux;

$$\dot{m}_{ox} = A_{ox} e^{\frac{-E_{ox}}{\mathcal{R}T_S}} \tag{36}$$

gives the mass flux and the regression rate of the fuel. With this mass flow, write the energy equation for this surface. Solving the energy equation for the surface temperature T_S gives it as a function of the nondimensional standoff distances ξ^*, the fraction of oxidizing reactants in the diffusion flame β_F and the properties of the fuel and oxidizer.

$$\begin{aligned} T_S = T_0 - \alpha\frac{h_{gas-ox}}{c_p} - (1-\alpha)\frac{h_{pyr-fuel}}{c_p} + \\ (1-\beta_F)\alpha[\frac{Q_{AP}}{c_p}e^{-\xi^*_{AP}} + \frac{Q_{FF}}{c_p}e^{-\xi^*_{FF}}] + \beta_F\frac{Q_{FF}}{c_p}e^{-\xi^*_{FF}} \end{aligned} \tag{37}$$

The FF subscript refers to the final diffusion flame and the AP subscript refers to the Ammonium Perchlorate flame. Beckstead, Derr, and Price also derive the necessary relations to determine the nondimensional standoff distances for the flames.

The dependence of this relation on the fraction β_F shows that these flames can be dominated by competition between the monopropellant flame and the main flame fr the oxidizer for a range of pressures. At low pressures it can be shown that the mixing flames are lower than the AP flame, causing all of the oxidizer to be combusted in the main flame. However, as the pressure (and thus recession rate) increases, the AP flame height decreases and the AP decomposition products begin to react alone until at high pressure almost none of the AP decomposition products react directly with the binder.

6.3.3 Heat Release in BDP Model

The flame temperatures of the flames can also be determined through energy balances of the products coming in once the surface temperature has been determined. Writing the conservation of energy for the AP flame:

$$Q_{AP} = c_p(T_{AP} - T_0) + Q_L \tag{38}$$

where Q_L is the heat of gasification of the oxidizer. This balance can also be written for the diffusion and primary (AP+Binder) flames:

$$Q_{FF} = \frac{c_p}{\alpha}(T_S - T_0) - \alpha(T_{AP} - T_0) + \frac{1-\alpha}{c_p}Q_{fuel} \tag{39}$$

$$Q_{PF} = c_p(T_f - T_0) + \alpha Q_L + (1-\alpha)Q_{fuel} \tag{40}$$

These equations can then be used to determine the various flame temperatures depending on the size and exact geometry of the problem.

6.3.4 Improvements to the BDP Model

One of the issues with the BDP model is that it does not address the edge burning between the AP and the binder in a very rigorous way, simply modeling it as a mixing dominated flame. A more accurate flame geometry is shown in figure 12. This replaces the mixing flame in the BDP model with a flame called a Leading Edge Flame (LEF). This flame is defined by a mixing zone below the flame and on top of the mixing zone a premixed flame where most of the heat release occurs. This creates fuel rich products that form a diffusion flame with the oxygen rich exhaust products from the AP flame.

Another important difference between this model and the BDP model is that this model has the binder in the middle of the sandwich as opposed to the oxidizer. Because a typical solid fuel is about 60-75% oxidizer by volume, this is a better approximation for a small region of of the propellant.

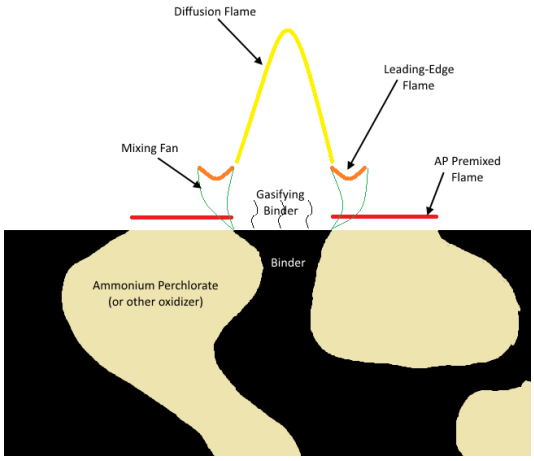

Fig. 12. Lee et.al. model of AP-Binder-AP flame, adapted from [17]

An important feature of the LEFs is their capacity to interact with each other at short binder distances [17]. This interaction, where each flame can add heat to the other flame, will increase the burning rate and flame temperature. However, if the binder becomes too thin the flame becomes fuel deficient and the flame temperature and burn rate begins to decrease again. The LEFs are very important due to their high heat release and their proximity to the surface, it is important to understand their interactions well. It is also important to not that because of the scale of these reactions, all the flames will interact in some capacity, and a more complete model can better understand the interconnections between the flames.

The position of these LEFs determines in large proportion the overall characteristics of the burning. Their hoirzontal placement is centered over the stoichiometric line between the oxidizer and the binder, where the gases are diffusing into each other in stoichiometric proportions. The vertical position is mainly governed by the pressure in the chamber. An increased pressure has the effect of increasing the gas phase reaction and thus the flame speed, causing the flame to lie closer to the surface.

7 Limitations of Common Models

The limitations of most models revolve around the fact that most of the flames must be modeled as a 3D process, which is very computationally intensive. The sandwich approximation is good at predicting the performance of a AP and binder sandwich, but it only has moderate utility when computing the heat release of a real particle. The 1D approximation works well for the AP flame ,because it simply sits on top of the AP surface, and as such is reasonably well-approximated by a 1D approximation. However, it is impossible in a 1D or 2D model to account for the curvature and irregular nature of the ammonium perchlorate grains and the resulting 3D flame structure.

Another limitation of most models is caused by the large difference in scales in order to fully model a combustion chamber. The AP grains are on the order of 10 to 100 microns, while the combustion chamber can be on the order of meters. This large difference in scale presents difficulties in studying how the large scale phenomenon like acoustics and changing chamber pressure interact with the structure of the flame and the burning characteristics.

Finally, the problem of developing 1D models becomes exponentially harder with the addition of additives like aluminum particles to the binder or even non-homogeneity in the oxidizer particle sizes.

In order to be able to predict more accurately the flame structure, it is necessary to develop a 3D model that can handle a 3D flame structure. It must additionally be scalable to handle different kinds of oxidizer, binder, and additive ratios , particle sizes, etc.

8 Computational Models of Solid Motor Combustion

The main method to be employed in more accurately modeling the combustion and flow field of a reacting sandwich of AP and binder is numerical simulation in either two or three dimensions. Because of the increased complexity of the 3D case and the existence of 3D CFD solvers for the 3D applications, this report will be restricted to the 2D or axisymmetric cases.

8.1 Surface Kinetics and Recession

Again taking the example case to be the the AP-binder-AP sandwich shown in Figure 10, we first consider the kinetics modeling set forth in [18]:

$$\mathrm{AP(X)} \longrightarrow \text{decomposition products (Z)} \tag{41}$$

$$\mathrm{Z} + \text{binder(Y)} \longrightarrow \text{final products} \tag{42}$$

In the case of constant density these global reactions are assumed to follow a form of the Arrhenius rate law of the form $R = BPXe^{\frac{E_{act}}{\mathcal{R}T}}$ where B is a preexponential factor, P is the pressure and X is the concentration in question. Upon the relaxation of the constant density assumption the rate dependence becomes a system of seven differential equations relating each species concentration and density.

In the solid phase, the heat transfer can be modeled using Fourier's Law.

$$\rho_s T_t = \frac{\lambda_s}{c_p} \nabla^2 T \tag{43}$$

The difference in properties between the binder and the AP can be accounted for by using a piecewise function where the demarcation line is set using a level set function $\psi(x,y)$ defined such that its zero marks the demarcation between the binder and AP. The solid-gas interface can be modeled using another level set function $\eta(x,y,t)$ where x and y are also

functions of time. Then, the equation

$$\eta_t + \eta_x \frac{dx}{dt} + \eta_y \frac{dy}{dt} = 0 \tag{44}$$

is also true and therefore the interface between the solid and the gas phase can be written as

$$\eta_t + r_b |\nabla \eta| = 0 \tag{45}$$

where r_b is the burning rate of the solid. r_b can be assumed to follow a simple pyrolysis law of the form $r_b = A(\frac{P}{P_0}^n) e^{\frac{E}{\bar{R}T_s}}$, though with different constants for the binder and AP.

8.2 Boundary Conditions

Across the solid/gas interface, the conservations laws can be used to determine any discontinuities in properties across the boundary. This paper will follow the notation convention in [18] and define $[\phi] = |\phi_s^+ - \phi_s^-|$. The first condition comes from the conservation of mass in the gas phase.

$$[\rho(\vec{v} \cdot \hat{n} + r_b] = 0 \tag{46}$$

The second boundary condition follows from the conservation of energy, where Q_s is defined as the heat release or absorption due to the surface reactions.

$$[\lambda \hat{n} \cdot \nabla T] = -Q_s \dot{m} \tag{47}$$

It also must be true that $[T] = 0$ due to Fourier's Law, and we can also define a fourth boundary condition based on the conservation of individual species.

$$\dot{m}[X_i] = [\rho D \hat{n} \cdot \nabla X_i], \quad i = X, Y, Z \tag{48}$$

8.3 Numerical Methods

Before simulation, all quantities are nondimensionalized by appropriate reference quantities in order to bring the scales of the simulation to a good scale for computation. Additionally, the pressure in the momentum equation can be rescaled since the pressure gradient, not the actual pressure, is what matters in the momentum balance. Since this process is quasi-unsteady, the pressure is broken down into a steady value and an unsteady portion. It is then possible to add a pseudo-derivative term to the conservation equation that causes it to converge faster while disappearing at the steady state.

With those steps in place to aid in numerical accuracy and speed convergence, a mesh of points is made and then solved on those equations using a second order solver. The periodic system can be solved as a system of Periodic Block-Tridiagonal Equations. Then, by performing approximations, the code can implicitly perform the final solution step and determine the solution at time n_+1 from the solution at n. The grid used in [18] is 140×70, just to give an idea of accurate grid sizes.

8.4 Solid Rocket Motor Modeling

In the modeling of a complete motor, considerations must be expanded to include fuel additives. The most common of these is solid aluminum particles. However, during combustion these will oxidize to create Al_2O_3, which will form particulates in the exhaust cloud which can take the form of alumina smoke and also larger solid particulates. Both of these products will reduce the overall I_{sp} of the engine because they will not expand with the flow as the flow goes through the nozzle, to give a first-order explanation. Therefore, it is important to understand the nature of these products formed. The larger solid particles can be analyzed with a Lagrangian (Control Mass) approach, while the smoke and gaseous combustion products can be analyzed from an Eulerian (Control Volume) perspective, resulting in a hybrid model [19].

In order to connect the two models, the assumption is made that many large particles in the simulation undergo similar conditions, and thus can be modeled with a single simulated Lagrangian particle simulation. Therefore, it is possible to model the large number of particles in the simulation with a much smaller number of actual simulations, reducing the computational cost significantly. It is then possible to write conservation equations for mass, energy, and momentum for the Eulerian volume and at the interfaces to connect the models. This is what constitutes the hybrid model.

With this framework in plac, mass, energy, ansd species conservation laws can be applied to the aluminum masses to determine their state as a function of time. The effect of the alumina smoke on the Eulerian continuum can be accounted for through a modification of the continuum state properties as a function of the mole fraction of solid alumina smoke and the bulk properties of both the surrounding gas and the alumina.

$$T = T(\rho_g, e_g, \rho_{Al}, e_{Al}, \alpha_{Al}) \tag{49}$$

$$\tilde{M} = \tilde{M}(\rho_g, e_g, \rho_{Al}, e_{Al}, \alpha_{Al}) \tag{50}$$

$$\gamma = \gamma(\rho_g, e_g, \rho_{Al}, e_{Al}, \alpha_{Al}) \tag{51}$$

Here e is defined as the specific internal energy of the phase. Turning to the modeling of the aluminum particles, which can be molten, we can use empirical correlations to model the combustion rate itsef in a straightforward manner. Another effect to consider is that, due to shear forces, these particles often breakup over the course of the flow. To determine both this breakup size distribution and the initial size distribution, we can write two probability density functions to govern the sizing of the particles up breakup and at formation. These probability models can be based on empirical correlations presented in reference [19] which are approximated as bi-model log-normal distributions. With this model in place to determine the effect of the aluminum on the com-

bustion, it is possible to run a numerical simulation of the combustion chamber with an appropriate mesh and numerical scheme, discussed earlier.

9 Summary of Research

Understanding the combustion of solid rocket propellant is useful for the development of solid rocket motors. In modeling the combustion of solid rocket propellant, the key predictions are:

1. The flame temperature, which affects the efficiency (I_{sp} and c^*) of the motor.
2. The composition (or average molar mass) of the exhaust, which affects the efficiency (I_{sp} and c^*) of the motor.
3. The propellant burning rate as a function of chamber pressure, which determines the equilibrium chamber pressure and the thrust of the motor.

Prediction of the flame temperature and exhaust composition is easily achieved with chemical equilibrium algorithms. Prediction of the burning rate, however, is more difficult and requires detailed models of the combustion process. In our investigation of the combustion process, we have chosen to focus on ammonium perchlorate composite propellant (APCP), which is a modern, commonly used propellant. Experiments with strand burners and rocket motors have largely characterized the pressure-burning rate relation of APCP, so ample data is available to verify combustion models. Composite propellant burns by decomposing vapors from solid oxidizer particles and from the surrounding polymer fuel. The oxidizer-rich and fuel-rich vapors mix by diffusion, and react at some distance from the solid surface. Early combustion models such as Beckstead, Derr, and Price (BDP) posit a conceptual explanation of the flame structure and provide 1-dimensional equations. Modern computation models employ 2- or 3-dimensional reacting flow simulations, and give a more rigorous description of the flame structure. In the analysis section of our project, we will implement a 1-dimensional simulation which predicts the flame temperature, exhaust composition, and burning rate of APCP. Our model will be loosely based on the BDP model, and will use Cantera to solve the chemical kinetics.

10 Development of Model

The model was developed in Python 2.7 using the Cantera Python plugin. The overall architecture of the model can be split into roughly three sections, the surface modeling, the heat transfer modeling, and the flame modeling itself. The flame structure is not modeled, but rather it is assumed from [15] that the AP flame is a line parallel to the AP surface and that the leading edge and final flames can be modeled as a parabolic surface with a weighted heat release. These are both symmetric around an assumed circular grain of AP. This is shown below in Figure 13.

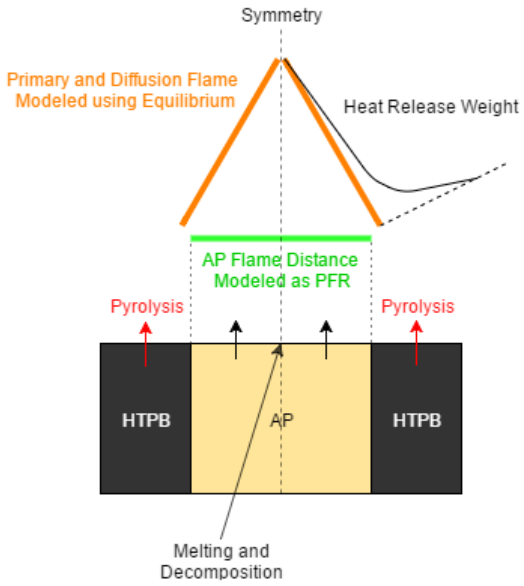

Fig. 13. A diagram of the model used to simulate the combustion of a grain of AP with a HTPB binder.

The surfaces are modeled using rate equations to determine the change in surface temperature and an ODE integrator to determine the change in surface temperature at a given time step. This is then coupled to an Arrhenius rate equation to determine pyrolysis or surface boil-off.
The heat transfer is modeled as an exponential function of the distance from the surface, as is done in [15]. The heat transfer between the flames is not currently modeled.
The flame modeling is done as a plug flow reactor in Cantera for the AP flame and as an mixture reacting to equilibrium in the case of the leading edge and final flames, as both are diffusion limited, not kinetics limited.

10.1 Surface Modeling

Because of the lack of condensed phase reactions, the HTPB surface is easier to model than the AP surface. The HTPB surface is modeled as an infinite surface downward, with a constant thermal conductivity and heat capacity. Thus, a heat flux into the surface can be assumed to cause a temperature distribution well approximated by an exponential function of the form $(T_s - T_0)e^{-\beta x} + T_0$. Where β is a shape parameter. Applying the conservation of enthalpy at the surface:

$$\frac{dh_{surf}}{dt} = 0 = \dot{q}_{in} - \dot{q}_{solid} - \Delta h_{pyro}\dot{m}'' \tag{52}$$

at the surface of the HTPB and then using Fourier's law to equate $\dot{q}_{solid}$ to $-\lambda\frac{\delta T}{\delta x}|_{x=0}$. It is then possible to determine β as:

$$\beta = \frac{\dot{q}_{surf} - \Delta h_{pyro}\dot{m}''}{\lambda(T_s - T_0)} \tag{53}$$

However, this assumes that the distribution follows the exponential profile, which is only true heat is flowing into the bulk, meaning $\beta > 0$. Applying the heat equation:

$$\frac{\lambda}{c_p \rho} \frac{d^2T}{dx^2} - \frac{\delta T}{\delta t} = 0 \tag{54}$$

$$\frac{\delta T}{\delta t} = \frac{\lambda}{c_p \rho} \beta^2 (T_s - T_0) + r\beta(T_s - T_0) \tag{55}$$

Here r is defined as the surface regression rate. The mass flux out of the surface due to pyrolysis can be modeled as a Arrhenius rate equation of the form

$$\dot{m}'' = e^{\frac{-E_a}{RT_s}} \tag{56}$$

If the heat flux is out of the solid, which equates to $\beta < 0$, the total enthalpy "stored" by the solid is instead used to back out the surface temperature derivative. The total enthalpy "stored" by the solid is

$$h''(T_s) = \rho c_p \int_0^\infty T(x) - T_0 \, dx. \tag{57}$$

which evaluates to $\rho c_p (T_s - T_0) \frac{1}{\beta}$. Substituting in the definition of β, taking the derivative of the resulting equation with respect to time, and rearranging gives the following formula for $\frac{\delta T_s}{\delta t}$:

$$\frac{\delta T_s}{\delta t} = -\frac{\dot{q}^2_{solid}}{2\rho c_p \lambda (T_s - T_0)} \tag{58}$$

For the modeling of the AP surface, the same approach was used, however the enthalpy balance used at the beginning to solve for β contains additional terms to account for the mass flux to the condensed phase. Although the evaporation from the liquid phase can be modeled as an Arrhenius rate equation, the AP sublimation is modeled just using the heat flux and a heat of sublimation. The condensed phase is modeled as infinitely thin so it can't contain any heat in order to simplify calculations.

10.2 Heat Transfer Modeling

The heat transfer is modeled as in [15], where the heat transfer between a flame and the surface below it follows the following relation:

$$Q_{trans} = Q_{rel} e^{-\xi^*_f} \tag{59}$$

where ξ^*_f is the nondimensional heat release standoff distance, defined as

$$\xi^*_f = \frac{c_p m_{ox}}{\lambda} (x^*_f + \bar{x}^*_D) \tag{60}$$

Here, x^*_f is the standoff distance of the flame in question and the $\bar{x}^*_D$ is the diffusional distance. This relation is used from each point on the curve that defines our flame, to determine the heat fluxes to both the AP and HTPB from the heat release at each point.

In order to determine the heat release at different points along the flame, and to also model the leading edge flame, each point on the flame curve has a weight that determines how much of the total heat release is released at that particular location. The distribution of weights is determined by a gamma function with shape parameter k and scale parameter θ chosen in order to match experimental data.

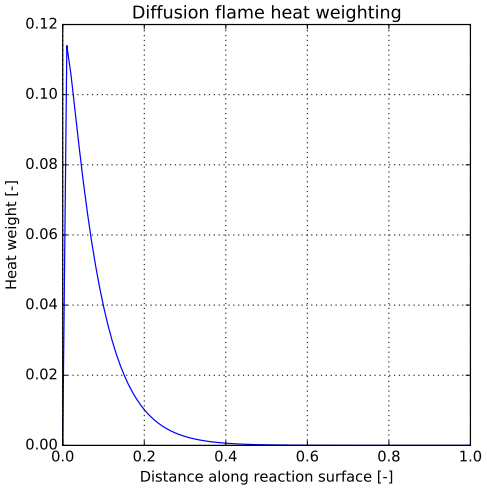

Fig. 14. The heat release weights. This weighting profile is a gamma function with shape 1.1 and scale 0.07.

As is mentioned before, the heat transfer between flames is not modeled. Qualitatively, if the heat transfer between flames were modeled, heat would move from the leading edge flame to the AP flame. Therefore, the temperature of the AP flame would increase, and thus decrease the distance from the AP flame to the surface. This would increase the heat flux to the AP surface, and decrease the heat flux to the HTPB surface, since some of the heat currently modeled as going from the leading edge flame to the HTPB would instead go to the AP flame. In the simulation, we encountered an issue where there was not enough heat going to the AP section to match experimental data. This was solved by decreasing our estimate of the enthalpy of vaporization of the AP from the value given by [15].

10.3 Flame Modeling

The flames are modeled differently based on the dominating mechanism in their combustion. For the AP flame, the limiting factor in the combustion is the kinetics, since it is premixed by definition as it sublimates off of the AP crystal. The leading edge flame and final flame are diffusion limited,

and therefore we can assume that what does react reacts to equilibrium since the kinetics are much faster than the diffusion in the high temperature environment.
Therefore, we model the AP flame using a plug flow reactor in order to determine the flame standoff distance analytically. However, for the leading edge and final flames, we simply equilibrate the output gas of the AP flame with the results of the HTPB decomposition and then distribute the heat according to the weighting function described in section 10.2. The heat release in both cases can then simply be described as the enthalpy difference between the starting and ending states.

10.3.1 Combustion Mechanism

The chosen combustion mechanism is listed in full in [20], where we use the combustion mechanisms for both the AP alone and the AP and HTPB. The AP decomposed gas consisted of 26% NH_3, 5% N_2O, 12% O_2, 17% H_2O, and 21% $HClO_4$ as per the approximation given in [21]. The combustion mechanism used here was for only AP and consisted of 22 reactions.
For the HTPB, the reaction mechanism used consisted of 76 reactions. The products of the HTPB pyrolysis were approximated to have been 100% C_4H_6, which is shown to be a good approximation in [22]. This input was fed, along with the products of the AP flame, into the equilibrium calculation to determine the leading edge flame temperature.

11 Results

11.1 Startup Transient

We used our software to simulate the startup transient of propellant combustion. We assume that the propellant begins at temperature of 300 K in an inert atmosphere pressurized to 6 MPa. The propellant is 86% AP and 14% HTPB by mass. The AP particle diameter is 50 µm, and is surrounded by a 2 µm wide ring of HTPB. Combustion is initiated by pulsing a Gaussian heat wave (30 MW m^{-2} peak, $1\sigma = 0.5$ ms) into the propellant surface. This setup is analogous to the combustion process in a strand burner test. In the physical system, the ignition heat pulse would be provided by a pyrotechnic squib or a laser.

Plots of the simulation outputs are shown in figure **??**. The ignition pulse is centered at 2 ms simulation time. Before ignition, the surface temperature is stable at 300 K and no mass flux is emitted from the surface. After the ignition transient ($t > 3.5$ ms), the heat fluxes, temperatures, and flame standoff distances stabilize to their stead-state values.

At the start of the ignition transient, the oxidizer and fuel surface temperatures rise due to the igniter heat flux, but no significant mass flux occurs ($t = 1.0 - -1.5$ ms, top-right plot). The fuel surface heats faster than the oxidizer surface. In our surface model, the temperature rise rate is inversely proportional to the product of heat capacity and thermal conductivity:

$$\frac{dT_S}{dt} \propto \frac{q_{to\_surface}}{c\lambda} \tag{61}$$

The dependence on heat capacity is obvious, but the effect of thermal conductivity is more subtle: if the thermal conductivity of the material is higher, heat flows from the surface into the bulk solid more quickly, so a greater thickness of the bulk solid must be heated in order to raise the surface temperature by the same amount. The ammonium perchlorate surface has a very low heat capacity (180 J kg^{-1} K^{-1}), typical of crystalline solids. The HTPB heat capacity is 2386 J kg^{-1} K^{-1}. However, the AP thermal conductivity exceeds that of HTPB (5.5 vs 0.22 W m^{-1} K^{-1}) by greater ratio. Therefore, $c\lambda$ is greater for AP than HTPB, and the AP surface heats up more slowly.

At $t \approx 1.6$ ms, the AP reaches its sublimation temperature (700 K) and the HTPB is hot enough that the pyrolysis reaction can progress at a significant rate. The mass fluxes of gas from each surface increase quickly, and the AP and leading edge flames start to burn this gas. Note that there is some ringing from numerical stability problems in our forward-Euler solver at this point.

The heat fluxes, mass fluxes, and temperatures peak at $t = 2$ ms, when the igniter heat flux peaks. After, the heat fluxes, mass fluxes, and temperatures begin to decrease to their steady state values.

One the igniter heat flux subsides, a self-sustaining combustion process continues.

The steady state values attained by our model match those reported by other researchers on similar propellant setups; see table 3. BDP [15] is a flame-structure-based numerical simulation, like ours. Gross & Beckstead simulate the combustion process with reacting flow Computational Fluid Dynamics software [23]. Rocket Propulsion Analysis is a chemical equilibrium solver [24].

Note that our flame standoff distances are similar to those of [15] but different from those of [23]. This is difference is due to our heat transfer models, our model is more similar to [15].

12 Burn rate vs Pressure

We ran our simulation at several pressures to explore our simulation's dependence on pressure. Our simulation accurately captures the effects of pressure on the surface regression rate, as illustrated by the comparison to Gross and Beckstead's data in figure 16. We fit a power law to our data to determine the parameters of equation 13,

$$r = ap^n$$

Table 3. Comparison of our simulation with previous works.

Simulation	Ours	BDP	Gross & Beckstead	RPA
Type	Structure-based	Structure-based	Reacting Flow CFD	Chemical Equilibrium Only
Conditions	$p_c = 6\,\mathrm{MPa}$ $FO_{mass} = 0.16$ $d_{ox} = 50\,\mu\mathrm{m}$	$p_c = 14\,\mathrm{MPa}$ $FO_{mass} = 0.42$ $d_{ox} = 20\,\mu\mathrm{m}$	$p_c = 6\,\mathrm{MPa}$ $FO_{mass} = 0.16$ $d_{ox} = 50\,\mu\mathrm{m}$	$p_c = 6\,\mathrm{MPa}$ $FO_{mass} = 0.16$ -
Heat flux to fuel surface	$75\,\mathrm{MW\,m^{-2}}$	-	$80\,\mathrm{MW\,m^{-2}}$	-
Heat flux to oxidizer surface	$40\,\mathrm{MW\,m^{-2}}$	-	$50\,\mathrm{MW\,m^{-2}}$	-
AP flame standoff distance	$3.0\,\mu\mathrm{m}$	$5\,\mu\mathrm{m}$	$0.2\,\mu\mathrm{m}$	-
Leading edge flame standoff distance	$11.5\,\mu\mathrm{m}$	$20\,\mu\mathrm{m}$	$1\,\mu\mathrm{m}$	-
Burn rate	$2.5\,\mathrm{cm\,s^{-1}}$	$1\,\mathrm{cm\,s^{-1}}$	$2.5\,\mathrm{cm\,s^{-1}}$	-
AP flame temperature	2050 K	1400 K	1370 K	-
Final temperature	3250 K	2545 K	3100 K	2804 K
Products	0.34 H_2O 0.18 HCl 0.14 CO_2 0.10 N_2 0.09 O_2 0.04 CO 0.04 OH 0.04 Cl	-	-	0.27 H_2O 0.26 HCl 0.18 CO_2 0.17 CO 0.10 N_2 0.01 Cl

and found $a = 2.83 \times 10^{-5}\,\mathrm{ms^{-1}Pa^{-n}}$ and $n = 0.437$. Accepted values for AP HTPB propellant are $a = 1.17 \times 10^{-5} - -1.40 \times 10^{-4}\,\mathrm{ms^{-1}Pa^{-n}}$ and $n = 0.40$ [1].

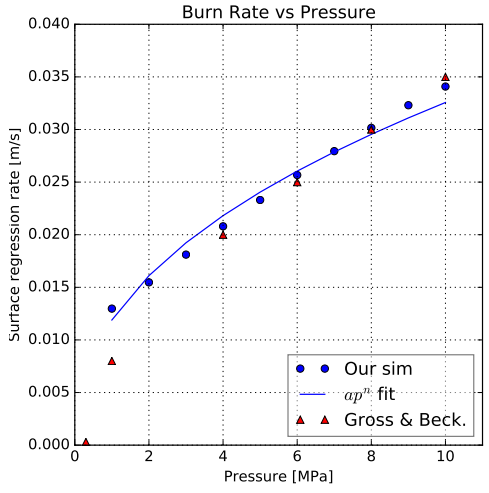

Fig. 16. Dependence of burn rate on pressure.

References

[1] Sutton, G. P., and Biblarz, O., 2010. *Rocket Propulsion Elements*, 8th ed. Wiley, Hoboken.

[2] Kubota, N., 2012. *Propellants and Explosives*, 2nd ed. Wiley-VCH, Weinheim.

[3] Bedard, A. Double base solid propellants.

[4] Chen, J. K., and Brill, T., 1991. "Chemistry and kinetics of hydroxyl-terminated polybutadiene (HTPB) and diisocyanate-HTPB polymers during slow decomposition and combustion-like conditions". *Combustion and Flame*.

[5] Narasimha, R., 1985. "Rockets in mysore and britian, 1750-1850 a.d.".

[6] McBride, B., Gordon, S., and Zehe, M., 2010. Chemical equilibrium with applications.

[7] Connell, T. L., Risha, G. A., Yetter, R. A., Roberts, C. W., and Young, G., 2015. "Boron and polytetrafluoroethylene as a fuel composition for hybrid rocket applications". *Journal of Propulsion and Power*.

[8] Guirao, C., and Williams, F. A., 1971. "A model for ammonium perchlorate deflagration between 20 and 100 atm". *AIAA Journal*.

[9] Price, C., Boggs, T., and Derr, R., 1978. "Modeling of solid monopropellant deflagration". *AIAA 16th Aerospace Sciences Meeting*.

[10] Tingfa, D., 1989. "Thermal decomposition studies of solid propellant binder HTPB". *Thermochemical Acta*.

[11] Klotx, S., Thynell, S. T., Huang, I. T., and Kuo, K. K., 1990. "Analysis of plumes of solid propellant combustion using an FT-IR spectrometer". *AIAA/SAE/ASME/ASEE 26th Joint Propulsion Conference*.

[12] Cohen, N. S., Fleming, R. W., and Derr, R. L., 1974. "Role of binders in solid propellant combustion". *AIAA Journal*.

[13] Ermolin, N. E., 1995. "Model for chemical reaction kinetics in perchloric acid - ammonia flames". *Combustion Explosion and Shock Waves*.

[14] Jacobs, P. W. M., and Whitehead, H. M., 1969. "Decomposition and combustion of ammonium perchlorate". *ACS Chemical Reviews*.

[15] Beckstead, M. W., Derr, R. L., and Price, C. F., 1970. "A model of composite solid-propellant combustion based on multiple flames".

[16] Jeppson, M. B., Beckstead, M. W., and Jing, Q., 1998. "A kinetic model for the premixed combustion of a fine AP/HTPB composite propellant.". *36th Aerospace Sciences Meeting and Exhibit AIAA*.

[17] Lee, S.-T., Price, E. W., and Sigman, R. K., 1994. "Effect of multidimensional flamelets in composite propellant combustion".

[18] Hegab, A. M., Sait, H. H., Hussain, A., and Said, A. S., 2014. "Numerical modeling for the combustion of simulated solid rocket motor propellant". *Computers and Fluids*.

[19] Shimada, T., Daimon, Y., and Sekino, N., 2007. "Numerical simulation of flow inside a solid rocket motor by eulerian-hybrid approach with relation to nozzle inlet ablation". *Experimental and Computational Aerothermodynamics of Interal Flows*.

[20] Goncalves, R. F. B., Ito, K., Machado, F. B. C., and Rocco, J. A. F. F., 2012. "Ammonium perchlorate and ammonium perchlorate - hydroxyl terminated polybutadiene simulated combustion". *Journal of Aerospace Technology Management*.

[21] Beckstead, M. W., Puduppakkam, K. V., and Yang, V., 2004. "Modeling and simulation of combustion of solid propellant ingredients using detailed chemical kinetics". *AIAA*.

[22] Cai, W., Thakre, P., and Yang, V., 2008. "A model of ap/htpb composite propellant combustion in rocket motor environments". *Combustion Science and Technology*.

[23] Gross, M. L., and Beckstead, M., 2011. "Steady-state combustion mechanisms of ammonium perchlorate composite propellants". *JOURNAL OF PROPULSION AND POWER,* **27**(5).

[24] Ponomarenko, A., 2015. Rocket propulsion analysis.